Pms2 and uracil–DNA glycosylases act jointly in the mismatch repair pathway to generate Ig gene mutations at A–T base pairs

Giulia Girelli Zubani,[1]* Marija Zivojnovic,[1]* Annie De Smet,[1] Olivier Albagli-Curiel,[2] François Huetz,[1,3] Jean-Claude Weill,[1] Claude-Agnès Reynaud,[1] and Sébastien Storck[1]

[1]Institut Necker-Enfants Malades, Institut National de la Santé et de la Recherche Médicale U1151, Centre National de la Recherche Scientifique UMR 8253, Faculté de Médecine-Site Broussais, Université Paris Descartes, Sorbonne Paris Cité, 75014 Paris, France
[2]Institut Cochin, Institut National de la Santé et de la Recherche Médicale U1016, Centre National de la Recherche Scientifique UMR8104, Faculté de Médecine-Site Cochin, Université Paris Descartes, Sorbonne Paris Cité, 75006 Paris, France
[3]Département d'Immunologie, Institut Pasteur, 75015 Paris, France

During somatic hypermutation (SHM) of immunoglobulin genes, uracils introduced by activation-induced cytidine deaminase are processed by uracil–DNA glycosylase (UNG) and mismatch repair (MMR) pathways to generate mutations at G–C and A–T base pairs, respectively. Paradoxically, the MMR-nicking complex Pms2/Mlh1 is apparently dispensable for A–T mutagenesis. Thus, how detection of U:G mismatches is translated into the single-strand nick required for error-prone synthesis is an open question. One model proposed that UNG could cooperate with MMR by excising a second uracil in the vicinity of the U:G mismatch, but it failed to explain the low impact of UNG inactivation on A–T mutagenesis. In this study, we show that uracils generated in the G1 phase in B cells can generate equal proportions of A–T and G–C mutations, which suggests that UNG and MMR can operate within the same time frame during SHM. Furthermore, we show that $Ung^{-/-}Pms2^{-/-}$ mice display a 50% reduction in mutations at A–T base pairs and that most remaining mutations at A–T bases depend on two additional uracil glycosylases, thymine–DNA glycosylase and SMUG1. These results demonstrate that Pms2/Mlh1 and multiple uracil glycosylases act jointly, each one with a distinct strand bias, to enlarge the immunoglobulin gene mutation spectrum from G–C to A–T bases.

INTRODUCTION

Affinity maturation of antibodies during T-dependent immune responses is the outcome of somatic hypermutation (SHM), a mutagenic process targeted at the Ig heavy and light chain V regions (Berek and Milstein, 1987). This process is triggered by activation-induced cytidine deaminase (AID), a cytidine deaminase that is preferentially active in B cells within germinal centers (GCs; Muramatsu et al., 2000; Revy et al., 2000). Mutations that accumulate in IgV genes become selected upon appropriate T helper signals during a complex process of cyclic trafficking between the dark zone of GCs, where mutagenesis and accelerated proliferation are considered to take place, and the light zone, where B cell prolifera-

tion slows down to allow for isotype switching and selection of variants with higher affinity (Victora and Nussenzweig, 2012; Gitlin et al., 2014, 2015).

Although AID initially deaminates cytidines, both G–C and A–T base pairs are equally mutated during SHM through distinct mechanisms (Rada et al., 2004). Transitions at G–C base pairs targeted by AID can be directly generated by replicative DNA polymerases if unrepaired uracils reach S phase. Alternatively, uracils can be converted by uracil–DNA glycosylase (UNG) into abasic sites that are subsequently bypassed by Rev1 and other translesion DNA polymerases to generate transversions as well as transitions at deamination sites (Jansen et al., 2006; Krijger et al., 2013). In contrast, mutations at A–T base pairs are introduced during an error-prone gap filling by DNA polymerase η (Zeng et al., 2001; Delbos et al., 2007), after its recruitment by monoubiquitinated proliferating cell nuclear antigen (PCNA; Langerak et al., 2007). These gaps are created by components of the mismatch repair (MMR) path-

way and the MutSα complex, composed of Msh2 and Msh6, which detects U:G mismatches and then activates 5′-3′ exonuclease I (ExoI; for review see Zanotti and Gearhart, 2016).

A paradox of SHM is that, in GC B cells, repair pathways are diverted from their usual antimutagenic activity to contribute to enlarging the mutation spectrum and to spreading mutations away from the initial deamination site (Di Noia and Neuberger, 2007). This abnormal behavior could be accounted for by the recruitment of these repair pathways outside their regular cell-cycle phase (Reynaud et al., 2009) and/or by the usage of alternative partners that could modify their biochemical properties. Correction of mismatches introduced during replication is performed by MMR during a very narrow window of time after the passage of the replication fork in eukaryotes (Hombauer et al., 2011). Indeed, at this precise moment, strand discontinuities that arose from leading- and lagging-strand synthesis, Okazaki fragment maturation, and removal of ribonucleotides are still present to direct MMR to the neosynthesized strand (Kunkel and Erie, 2015). Such nicks enable activation of the latent endonuclease activity of the MutLα complex Pms2/Mlh1, which creates multiple incisions on the discontinuous strand used as entry points for ExoI to generate a gap and remove the mismatched base (Kadyrov et al., 2006; Pluciennik et al., 2010; Goellner et al., 2015). Outside S phase, when these strand discontinuities are no longer available, there is evidence that MMR can function in a noncanonical, promutagenic fashion in nonreplicating cells exposed to complex DNA damages, with Msh2/Msh6 inducing the ubiquitination of PCNA and the recruitment of Pol η to damaged chromatin (Zlatanou et al., 2011; Peña-Diaz et al., 2012).

A–T mutagenesis by Pol η during SHM has obvious similarity with this noncanonical MMR (ncMMR) process (Bak et al., 2014; Zanotti and Gearhart, 2016). Yet, a major question is how the detection of the U:G mismatch is translated into a single-strand nick, required for subsequent DNA resection and error-prone synthesis by Pol η. Indeed, although Pms2 and Mlh1 are strictly required for canonical MMR in vivo, both are surprisingly dispensable for SHM (Frey et al., 1998; Phung et al., 1999; Ehrenstein et al., 2001; van Oers et al., 2010; Chahwan et al., 2012). One possible scenario, given that AID is a processive enzyme (Pham et al., 2003), is based on the occurrence of clustered cytidines deaminated simultaneously: as a consequence, while Msh2/Msh6 detects a U:G mismatch, a second uracil may be processed by UNG and an apurinic/apyrimidinic endodeoxyribonuclease (APEX) to generate the required nick. This scenario, proposed by Schanz and colleagues, is supported both by in vitro (Schanz et al., 2009) and in vivo (Stavnezer et al., 2014; Zivojnovic et al., 2014) data, but it fails to explain the low impact of UNG inactivation on A–T mutagenesis (Rada et al., 2002). Moreover, this scenario requires that UNG and MMR process uracils simultaneously during the same phase of the cell cycle, whereas some models proposed a temporal dissociation of both pathways (Weill and Reynaud, 2008; Liu and Schatz, 2009; Li et

al., 2013) to explain the relative independence of G-C and A-T mutagenesis observed in single knockouts for *Msh2* or *Ung* (Rada et al., 1998, 2002; Imai et al., 2003). Although mutations at G-C base pairs were shown recently to depend on excision of uracils during the G1 phase of the cell cycle (Sharbeen et al., 2012), it is not clear at present in which phase A-T mutagenesis proceeds.

Therefore, in this study, we first restricted AID expression to the G1 phase of the cell cycle in GC B cells in vivo to show that uracils produced in the G1 phase can indeed be substrates for both UNG and MMR pathways. Then, we show that mice with combined Ung/Pms2 deficiency display a 50% reduction in mutations at A–T base pairs, which proves for the first time that the Pms2/Mlh1 complex participates in hypermutation by providing the nick required for A–T mutagenesis. Its contribution has been so far unappreciated because UNG can fully compensate for its absence. Finally, using an in vivo RNA interference (RNAi) strategy, we show that mutations at A–T base pairs that persist in $Ung^{-/-}Pms2^{-/-}$ mice are generated through the action of two additional uracil glycosylases, TDG (thymine–DNA glycosylase) and SMUG1 (single-strand–selective monofunctional uracil–DNA glycosylase 1).

RESULTS
Restriction of AID expression to the G1 phase in vivo
To restrict AID expression to either the G1 or S/G2/M phase of the cell cycle, we fused the C terminus of AID to mKO2-hCDT1 or to mCherry-geminin fluorescent ubiquitination-based cell cycle indicators, respectively (Fucci; Sakaue-Sawano et al., 2008). We also generated mutant versions, in which the sites that regulate proteasomal degradation were ablated, to control for the functionality of the AID fusion protein. This was achieved by mutating the cyclin box that targets hCDT1 phosphorylation-directed degradation (RRL to AAA within the [65]PARRRLRL[72] cyclin/Cdk–binding consensus site of the protein; Liu et al., 2004) and, for geminin, by deleting the 9–amino acid destruction box ([33]RRTLKVIQP[41]), which abolishes APC/C-mediated ubiquitination at the M/G1 transition (McGarry and Kirschner, 1998).

Each construct was cloned in the internal ribosomal entry site (IRES)–containing bicistronic retroviral pMIG vector (Pear et al., 1998) to allow simultaneous expression of AID fusion proteins and enhanced GFP (EGFP) fluorescent reporter from the potent mouse stem cell virus long-terminal repeat promoter. Bone marrow hematopoietic stem cells (HSCs) from AID-deficient mice were transduced with these retroviral vectors and introduced into Rag2-deficient mice to restore their lymphoid compartment. Transduction efficiency of HSCs in vitro ranged from 20 to 40%, and peripheral reconstitution, estimated 2–3 mo later in the spleen, showed that EGFP^{+} cells represented 5–15% of total spleen cells, with a comparable distribution within the B and T cell compartments for all constructs (not depicted).

The cell-cycle restriction of AID fusion proteins was assessed on HSCs kept in culture 3 d after transduction in vitro
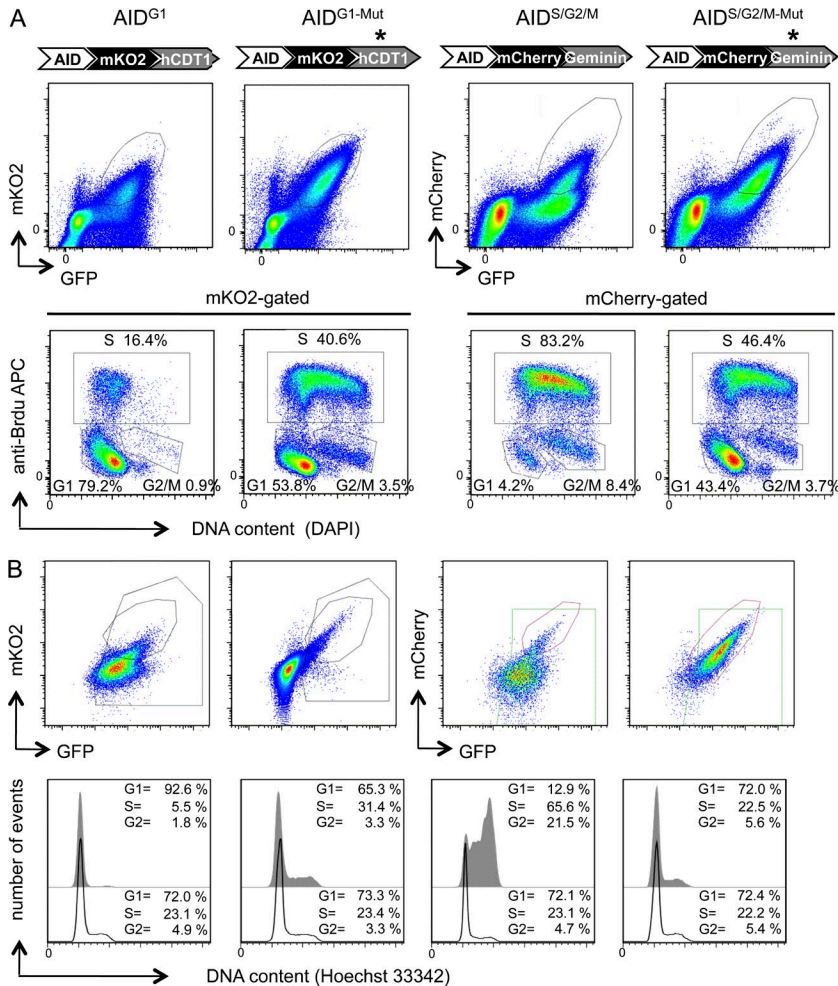
Figure 1. **Cell cycle–restricted expression of AID in transduced HSCs and ex vivo B cell blasts.** (A) Retroviral constructs expressing the G1-restricted form of AID fused to the mKO2 fluorescent reporter (AID-mKO2-hCDT1; AID[G1]) and its cell-cycle control mutant (represented by an asterisk; AID[G1-Mut]) or the S/G2/M-restricted form (AID-mCherry-geminin; AID[S/G2/M]) and its cell-cycle control mutant (asterisk; AID[S/G2/M-Mut]) linked to an IRES-EGFP reporter were used to transduce Lin⁻ HSCs. Cell-cycle analysis was performed 3 d after transduction and 30 min after BrdU addition, with DAPI staining to estimate the cell DNA content and anti-BrdU antibodies to identify cells undergoing replication. The distribution within the different phases of the cell cycle was estimated by FlowJo software. The FACS profiles are representative of two different transduction experiments with the four constructs. (B) Cell-cycle analysis of naive splenic B cells from restored animals, 3 d after LPS + IL-4 stimulation. Activation was performed on sorted EGFP⁺B220⁺GL7⁻PNA^low B cells for AID-mKO2-hCDT1 and AID-mCherry-geminin, mutated or not, and on total naive B cells for mutated AID-mKO2-hCDT1. Cell-cycle phases of EGFP⁺ cells were determined by quantification of DNA content through Hoechst staining. The cell-cycle profile of total EGFP⁺ B cells (bottom) and mKO2/EGFP or mCherry/EGFP double-positive cells (top) is shown, with distribution within the different phases of the cell cycle estimated by FlowJo software. FACS profiles are representative of two to three different experiments for each construct.

(Fig. 1 A) and further confirmed on ex vivo splenic B cell blasts obtained from restored animals after stimulation with LPS and IL-4 (Fig. 1 B). For the mutant vectors, transduced HSCs coexpressed EGFP and mKO2 or mCherry, with double-expressing cells on the diagonal of the FACS plot (Fig. 1 A). In contrast, for vectors with cell-cycle restriction, two populations could be distinguished: an EGFP-only subset and a double EGFP⁺mKO2⁺ or EGFP⁺mCherry⁺ population. In this case, according to Hoechst staining and BrdU incorporation, ∼79% of mKO2-positive cells were in the G1 phase, as compared with 43–54% for the mutated controls (Fig. 1 A). In agreement with the initial description of this restriction system, the non-G1 cells were in the early S phase (Sakaue-Sawano et al., 2008). For mCherry-expressing cells, 92% were in S/G2/M, which indicates, for both vectors, that appropriate restriction to the corresponding phase of the cell cycle was achieved in HSCs. Conversely, restriction was abolished by the mutations introduced in the hCDT1 and geminin peptides. Regarding ex vivo B cell blasts, although the overall mKO2 or mCherry fluorescence intensity was lower than in HSCs analyzed early after transduction, cells positive for AID-mKO2-hCDT1 or AID-mCherry-geminin showed the ex-

pected cell-cycle restriction, which was completely abolished in cells that expressed the mutant construct (Fig. 1 B). Therefore, AID restriction to G1 phase or S/G2/M was quite tight in vitro and perfectly maintained in mature B cells differentiated in vivo from transduced precursors. We also noted that the accumulation of AID-mKO2-hCDT1 or AID-mCherry-geminin was lower than that of mutant controls, a likely consequence of their cyclic degradation (Fig. 1, A and B). The fusion proteins and the cells that express them are hereafter referred to as AID[G1] (AID-mKO2-hCDT1), AID[G1-Mut], AID[S/G2/M] (AID-mCherry-geminin), and AID[S/G2/M-Mut].

G1-restricted AID generates the complete spectrum of mutations at the Ig locus

After 2 mo of lymphoid reconstitution with transduced HSCs, mice were immunized by intraperitoneal sheep RBC (SRBC) injection; GL7⁺ peanut agglutinin (PNA)^high EGFP⁺ GC B cells were sorted 2 wk later, and mutations in the J_H4 intronic region were determined for both AID-expression vectors (Fig. 2).

Mutation frequency induced by the control AID-fusion constructs was altogether low, with a threefold dif-
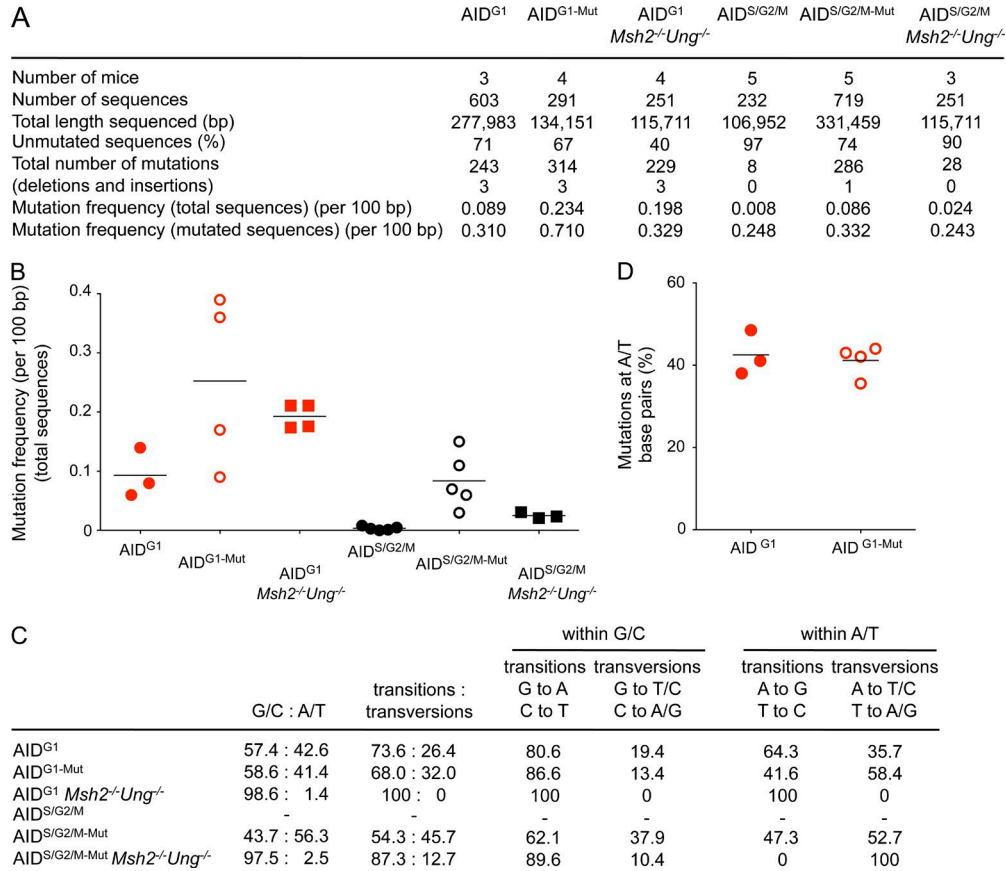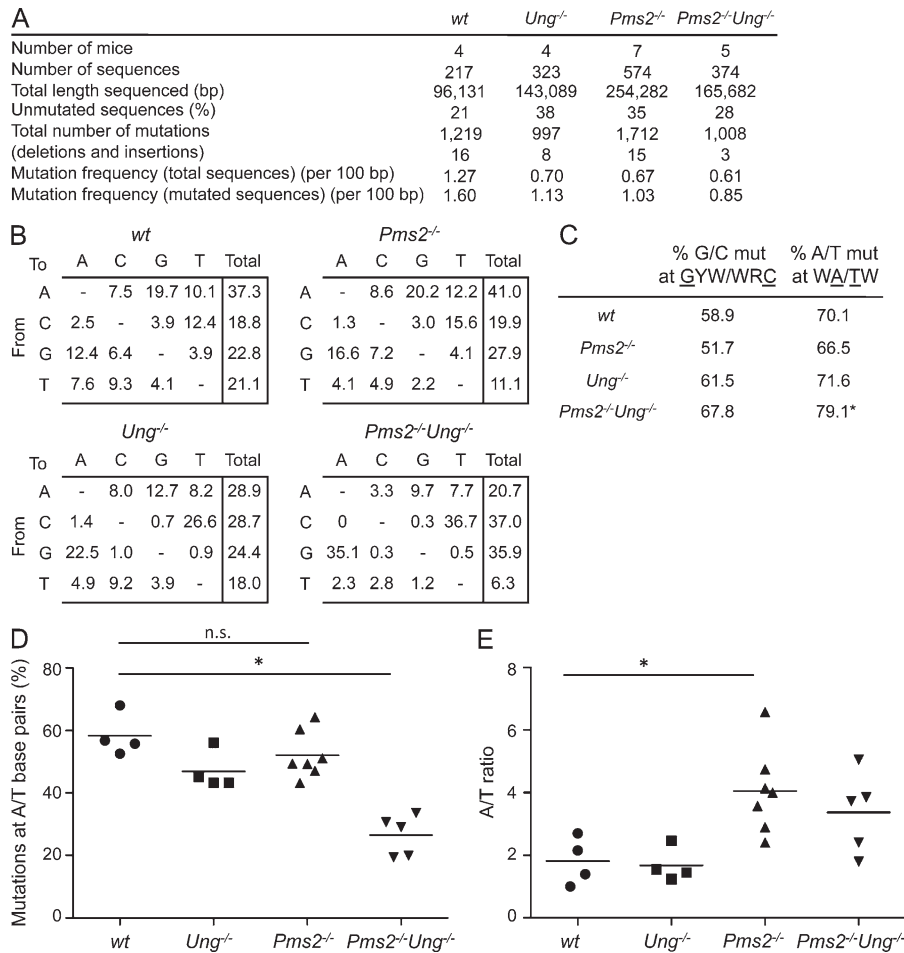
A

	AID^G1	AID^G1-Mut	AID^G1 Msh2^-/-Ung^-/-	AID^S/G2/M	AID^S/G2/M-Mut	AID^S/G2/M Msh2^-/-Ung^-/-
Number of mice	3	4	4	5	5	3
Number of sequences	603	291	251	232	719	251
Total length sequenced (bp)	277,983	134,151	115,711	106,952	331,459	115,711
Unmutated sequences (%)	71	67	40	97	74	90
Total number of mutations	243	314	229	8	286	28
(deletions and insertions)	3	3	3	0	1	0
Mutation frequency (total sequences) (per 100 bp)	0.089	0.234	0.198	0.008	0.086	0.024
Mutation frequency (mutated sequences) (per 100 bp)	0.310	0.710	0.329	0.248	0.332	0.243

C

	G/C : A/T	transitions : transversions	within G/C		within A/T	
			transitions G to A C to T	transversions G to T/C C to A/G	transitions A to G T to C	transversions A to T/C T to A/G
AID^G1	57.4 : 42.6	73.6 : 26.4	80.6	19.4	64.3	35.7
AID^G1-Mut	58.6 : 41.4	68.0 : 32.0	86.6	13.4	41.6	58.4
AID^G1 Msh2^-/-Ung^-/-	98.6 : 1.4	100 : 0	100	0	100	0
AID^S/G2/M	-	-	-	-	-	-
AID^S/G2/M-Mut	43.7 : 56.3	54.3 : 45.7	62.1	37.9	47.3	52.7
AID^S/G2/M-Mut Msh2^-/-Ung^-/-	97.5 : 2.5	87.3 : 12.7	89.6	10.4	0	100

Figure 2. **G1–restricted AID generates the complete spectrum of A–T and G–C mutations at the Ig locus.** (A) Mutation frequency in J_H4 intronic sequences of splenic GC B cells from Rag2-deficient animals restored with $Aicda^{-/-}$ and $Aicda^{-/-} Msh2^{-/-} Ung^{-/-}$ HSCs transduced with different AID-expressing vectors and immunized with SRBCs. (B) Representation of mutation frequencies from individual animals. Mutation frequencies in A are based on total sequences, whereas they are represented per individual mouse in B. (C) Base substitution pattern in J_H4 intronic sequences from the reconstituted animals. Values for AID^S/G2/M, which correspond to eight mutations in total, are not represented. (D) Percentage of mutations at A–T base pairs obtained for the individual AID^G1 and AID^G1-Mut restored mice. All individually analyzed mice (three to five for each type of construct per HSC genotype) are included in this figure.

ference between AID^G1-Mut and AID^S/G2/M-Mut restored cells, likely reflecting the different impact of the degron–fluorochrome fusion on AID activity (Fig. 2, A and B). In both cases, the ratio of G–C to A–T targeting was normal (Fig. 2 D), with a bias for transitions at G–C base pairs for AID^G1-Mut, which suggests that these AID C-terminal fusions may partially interfere with uracil glycosylase recruitment or base excision efficiency.

Restriction of AID expression to the G1 phase yielded a mutation frequency threefold lower than in the nonrestricted control (Fig. 2, A and B), a difference that likely corresponds to the lower accumulation of a protein that undergoes recurrent cell-cycle degradation (Fig. 1). However, AID^G1 cells displayed a similarly equilibrated proportion of mutations at G–C and A–T bases (Fig. 2, C and D), and this balanced ratio remained the same, whatever the stringency of the criteria used to eliminate clonal relationships, an important issue when analyzing small GC B cell samples (see the Immunization, genomic DNA extraction, and sequence analysis section

of Materials and methods). This indicates that uracils generated in G1 are substrates not only for the UNG-driven G/C SHM pathway as described previously (Sharbeen et al., 2012), but also for the Msh2-driven A/T SHM pathway.

In contrast, a negligible number of mutations over background was generated when AID was restricted to the S/G2/M phase (Fig. 2, A–C). To assess whether this minimal mutation load could result from a preferential error-free repair in this phase of the cell cycle, we transduced the same cell cycle–restricted AID constructs in HSCs from triple-deficient $Aicda^{-/-} Ung^{-/-} Msh2^{-/-}$ mice. Mutation frequency showed a similar two- to threefold increase for both AID^G1 and AID^S/G2/M, indicating a similar impact of error-free repair throughout the cell cycle (Fig. 2). Thus, the very low mutation frequency observed for our AID^S/G2/M construct is possibly linked, in addition to the lower efficiency of the AID^S/G2/M-Mut control compared with AID^G1-Mut, to the limited accumulation of its cell cycle–restricted form after each degradation cycle.

A

	wt	Ung−/−	Pms2−/−	Pms2−/−Ung−/−
Number of mice	4	4	7	5
Number of sequences	217	323	574	374
Total length sequenced (bp)	96,131	143,089	254,282	165,682
Unmutated sequences (%)	21	38	35	28
Total number of mutations	1,219	997	1,712	1,008
(deletions and insertions)	16	8	15	3
Mutation frequency (total sequences) (per 100 bp)	1.27	0.70	0.67	0.61
Mutation frequency (mutated sequences) (per 100 bp)	1.60	1.13	1.03	0.85

B

wt

From \ To	A	C	G	T	Total
A	-	7.5	19.7	10.1	37.3
C	2.5	-	3.9	12.4	18.8
G	12.4	6.4	-	3.9	22.8
T	7.6	9.3	4.1	-	21.1

Pms2−/−

From \ To	A	C	G	T	Total
A	-	8.6	20.2	12.2	41.0
C	1.3	-	3.0	15.6	19.9
G	16.6	7.2	-	4.1	27.9
T	4.1	4.9	2.2	-	11.1

Ung−/−

From \ To	A	C	G	T	Total
A	-	8.0	12.7	8.2	28.9
C	1.4	-	0.7	26.6	28.7
G	22.5	1.0	-	0.9	24.4
T	4.9	9.2	3.9	-	18.0

Pms2−/−Ung−/−

From \ To	A	C	G	T	Total
A	-	3.3	9.7	7.7	20.7
C	0	-	0.3	36.7	37.0
G	35.1	0.3	-	0.5	35.9
T	2.3	2.8	1.2	-	6.3

C

	% G/C mut at GYW/WRC	% A/T mut at WA/TW
wt	58.9	70.1
Pms2−/−	51.7	66.5
Ung−/−	61.5	71.6
Pms2−/−Ung−/−	67.8	79.1*

D

E

Figure 3. **Contribution of Pms2 to A–T mutagenesis is revealed in Pms2 × UNG–deficient mice.** (A) Analysis of mutations in J_H4 intronic sequences from Peyer's patch GC B cells of *WT*, *Ung−/−*, *Pms2−/−* (taken from Zivojnovic et al., 2014), and *Pms2−/− Ung−/−* mice. (B) Pattern of nucleotide substitution in the four genotypes (percentage) corrected for base composition. (C) Percentage of mutations within AID (GYW/WRC) or Pol η (WA/TW) mutation hotspots. G/C bases within GYW/WR(C) hotspots represent 18.6% of all G/C bases within the J_H4 sequence analyzed and, for A/T bases within WA/TW Pol η hotspots, 51.3%. A significant difference was observed for the frequency of WA/TW hotspots taken from individual double-knockout compared with *WT* mice. (D) Mutations at A-T base pairs (percentage). (E) A-over-T mutation ratios for *WT*, *Ung−/−*, *Pms2−/−*, and *Pms2−/−Ung−/−* mice. *, P = 0.0159; two-tailed Mann-Whitney *U* test. All individually analyzed mice (four to seven for each genotype) are included in this figure.

Nevertheless, our results clearly demonstrate that AID expression in the G1 phase can generate the complete spectrum of mutations observed in normal conditions at the Ig locus, and therefore, these data are fully compatible with a model in which UNG and MMR would operate within an identical time frame and would be able to cooperate to generate the single-stranded gaps required for mutagenesis at A–T base pairs.

Ung−/− Pms2−/− mice display a 50% reduction of SHM at A–T base pairs

A cooperative model between UNG and MMR is at odds with the modest reduction of mutations observed at A–T base pairs in *Ung−/−* mice (Fig. 3; Rada et al., 2002), but other enzymes may be involved and compensate for UNG absence to generate the nick required for ExoI entry. One candidate is the bona fide endonuclease of the MMR pathway, the Pms2/Mlh1 MutLα complex, whose activity in SHM may be masked in the presence of UNG and APEX.

To test this hypothesis, we crossed *Pms2−/−* mice with *Ung−/−* mice to generate double-deficient *Ung−/−Pms2−/−* animals and compared their SHM pattern in the nonselected J_H4 intronic sequence to that of WT and single-knockout mice.

In GC B cells isolated from Peyer's patches, the proportion of mutations at A–T base pairs, which reached 52 and 47% for *Pms2−/−* and *Ung−/−* mice, respectively, dropped to 27% in double-deficient mice, which corresponds to an ∼50% reduction of normal A–T mutation levels (Fig. 3 D). This reduction was even more pronounced in splenic GC B cells from mice immunized with SRBC 2 mo after bone marrow reconstitution (21% residual mutations at A–T base pairs; see Fig. 5 C). A–T to G–C transitions, the footprint of Pol η error-prone polymerization, were still predominant among A–T mutations in *Ung−/−Pms2−/−* mice, with a slight increase in mutations at its WA and TW hotspots, these data being in accordance with the observation that this enzyme is the sole contributor to A–T mutagenesis under physiological conditions (Fig. 3, B and C; Delbos et al., 2007). *Ung−/−Pms2−/−* also retained an enhanced A over T mutation ratio (a ratio of 3.4; Fig. 3 E), similar to that observed previously in *Pms2−/−* mice and different from the ratio of 1.8 observed in WT conditions. This ratio is close to the intrinsic T over A mutation bias of Pol η when copying the transcribed strand (a fourfold higher mutation frequency when copying T's compared with A's), which led us to conclude that, in the absence of Pms2, error-prone synthesis was restricted to the coding strand (Zivojnovic et al., 2014).

Overall, these data indicate that both Pms2 and UNG contribute to triggering MMR-dependent A–T mutagenesis, but because approximately half of mutations at A–T bases are still generated in double-deficient mice, one or several enzymes must play a backup role in this pathway.

TDG and SMUG1 can support A–T mutagenesis at the Ig locus

In addition to UNG, three mammalian enzymes possess uracil-DNA glycosylase activity (Visnes et al., 2009): SMUG1, TDG, and MBD4 (methyl-CpG–binding domain 4). Among these, only SMUG1 has been shown to play a backup role in SHM; although its knockout alone does not affect SHM pattern, the combined deficiency in UNG and SMUG1 leads to a 27% decrease in A–T mutagenesis (Dingler et al., 2014). MBD4 loss of function does not impact SHM on its own (Bardwell et al., 2003), but it has not been studied in an *Ung*-knockout context. The implication of TDG has not been explored so far, owing to its requirement for early embryonic development (Cortázar et al., 2011).

We measured by quantitative RT-PCR (qRT-PCR) the amount of *Smug1*, *Tdg*, and *Mbd4* transcripts in splenic GC B cells and naive B cells from immunized WT and $Ung^{-/-}Pms2^{-/-}$ mice (Fig. 4). Whereas *Mdb4* and *Tdg* are up-regulated in WT GC B cells 8.2 and 3.1 times, respectively, *Smug1* is slightly down-regulated (40% decrease) in GC compared with naive B cells, and its absolute level of expression is much lower than that of *Mdb4* and *Tdg* (Fig. 4, A and B). The levels of these transcripts remained unchanged in $Ung^{-/-}Pms2^{-/-}$ GC and naive B cells compared with WT (Fig. 4, A and B).

To test the capacity of SMUG1, TDG, and MBD4 to support A–T mutagenesis in the absence of UNG and Pms2, we developed a strategy of RNAi in vivo. This strategy consisted of reconstituting the lymphoid compartment of Rag2-deficient mice with $Ung^{-/-}Pms2^{-/-}$ HSCs transduced with retroviral vectors coding for microRNA-adapted shRNA (shRNAmir) against each target. We modified the pMIG vector used for AID restriction by replacing the IRES-EGFP sequence with a cassette that contains mouse 5′ and 3′ miR-155 flanking sequences embedded in the 3′ untranslated region of emerald GFP (EmGFP); hence, shRNAmir sequences cloned within this cassette are co-transcribed with EmGFP, which enables easy tracking and sorting by FACS of cells that express a high level of shRNAmir. 5–10 different hairpin sequences were screened for each target in 3T3 cells. We selected one (for *Mbd4* and *Smug1*) or two (for *Tdg*) shRNAmir that conferred knockdown efficiency >80% in 3T3 cells to conduct HSC transduction and lymphoid reconstitution of mice. After a single immunization with SRBCs, the efficiency of in vivo knockdown was determined for each animal by comparing the residual amount of target mRNA in sorted splenic GFP⁺ and GFP⁻ GC B cells, and the pattern of SHM of J_H4 intron was studied on DNA extracted from the same GFP⁺
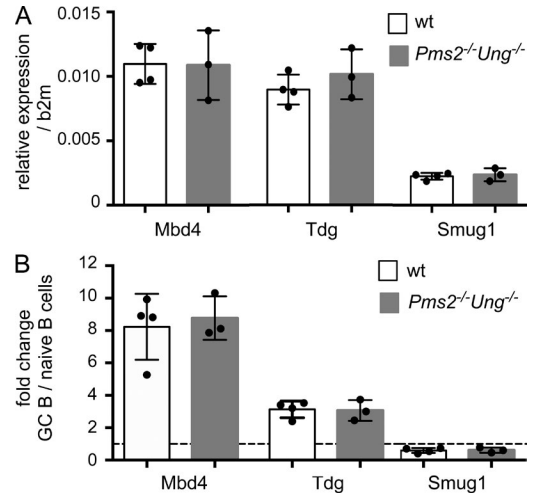
Figure 4. **Analysis of uracil glycosylase expression levels by qRT-PCR.** (A) Relative expression levels of *Mbd4*, *Tdg*, and *Smug1* in naive B cells (B220⁺GL7⁻CD95⁻) from spleen of immunized WT (n = 4) and $Ung^{-/-}Pms2^{-/-}$ (n = 3) mice, compared with β-2 microglobulin (b2m). (B) Relative expression of *Mbd4*, *Tdg*, and *Smug1* in GC B cells (B220⁺GL7⁺CD95⁺) compared with naive B cells from spleens of WT (n = 4) and $Ung^{-/-}Pms2^{-/-}$ (n = 3) mice. The dotted line represents a ratio of 1 between GC and naive B cells. Quantification was performed in triplicates for RNA samples from three to four different mice. Error bars represent SD.

GC B cells. On rare occasions, when too few GC B cells were isolated to perform qRT-PCR studies, the knockdown efficiency was measured on GFP⁺ and GFP⁻ naive B cells, as the knockdown values were well correlated between the two B cell compartments in control samples (not depicted).

Potent in vivo silencing of *Tdg*, ranging from 80 to 92%, was obtained with two different shRNAmir sequences (Fig. 5). TDG is apparently dispensable for B cell development and activation, as its inhibition in WT or in $Ung^{-/-}Pms2^{-/-}$ cells did not alter B cell reconstitution and GC reaction (not depicted), and its silencing had neither quantitative nor qualitative impact on SHM in WT GC B cells (Fig. 5). In contrast, it modestly but significantly decreased SHM at A–T base pairs in an $Ung^{-/-}Pms2^{-/-}$ background (16.7 vs. 21%; Fig. 5 C). *Mbd4* knockdown in $Ung^{-/-}Pms2^{-/-}$ did not affect A–T mutagenesis, but it should be noted that the repression of *Mbd4* was mild (from 57 to 69% in GC B cells). In accordance with the phenotype of $Smug1^{-/-}Ung^{-/-}$ cells (Dingler et al., 2014), A–T mutations dropped to 14.3% in $Ung^{-/-}Pms2^{-/-}$ GC B cells that expressed an shRNAmir against *Smug1* (Fig. 5 C). However, in our case, this difference was not statistically significant, most likely because RNAi is somewhat heterogeneous between mice. Nonetheless, when *Smug1* and *Tdg* shRNAmir sequences were concatenated in the same retroviral vector to drive simultaneous silencing of both genes in $Ung^{-/-}Pms2^{-/-}$ mice, A–T mutation frequency became extremely low (8 vs. 21% for nontransduced $Ung^{-/-}Pms2^{-/-}$ B cells and vs. 16.7% for *Tdg*-silenced B cells; Fig. 5 C).
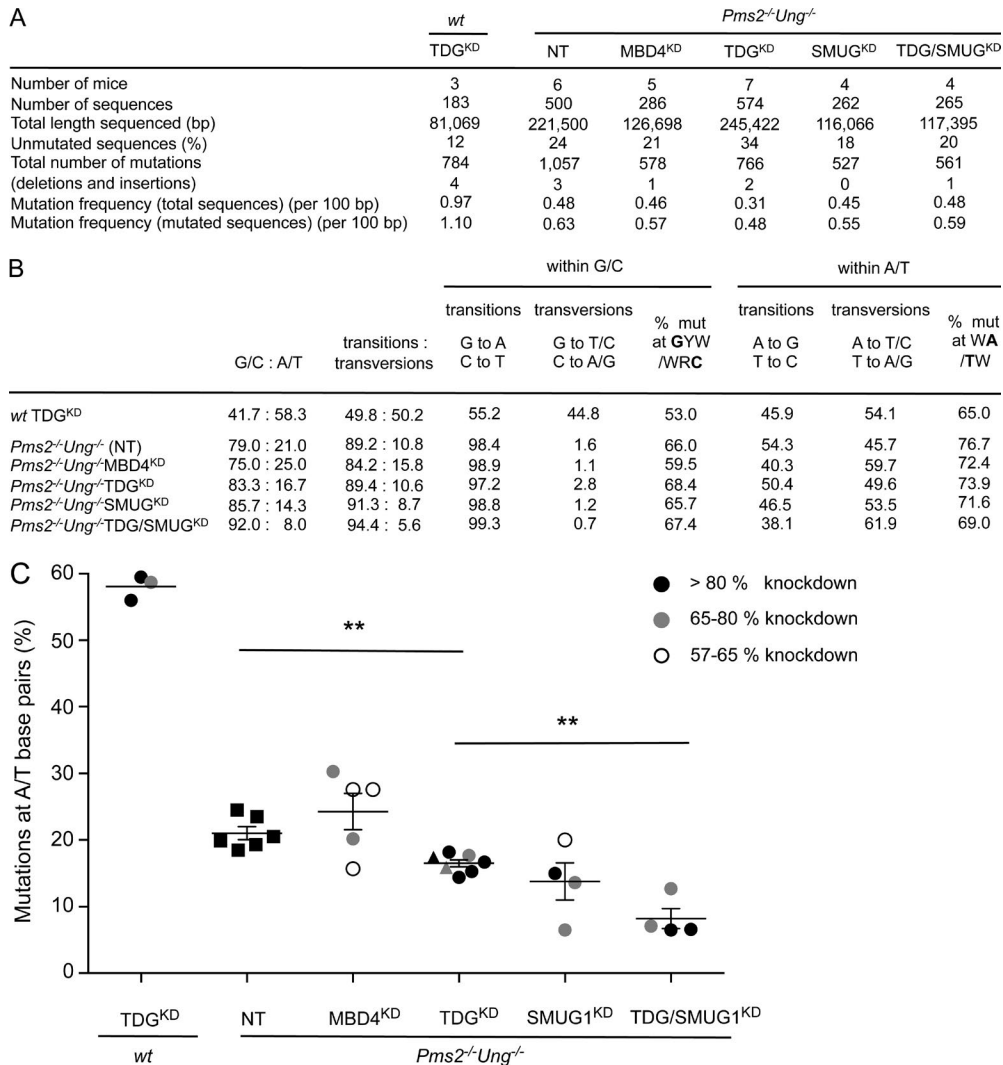
A

	wt	*Pms2^−/−Ung^−/−*				
	TDG^KD	NT	MBD4^KD	TDG^KD	SMUG^KD	TDG/SMUG^KD
Number of mice	3	6	5	7	4	4
Number of sequences	183	500	286	574	262	265
Total length sequenced (bp)	81,069	221,500	126,698	245,422	116,066	117,395
Unmutated sequences (%)	12	24	21	34	18	20
Total number of mutations	784	1,057	578	766	527	561
(deletions and insertions)	4	3	1	2	0	1
Mutation frequency (total sequences) (per 100 bp)	0.97	0.48	0.46	0.31	0.45	0.48
Mutation frequency (mutated sequences) (per 100 bp)	1.10	0.63	0.57	0.48	0.55	0.59

B

			within G/C			within A/T		
			transitions	transversions	% mut	transitions	transversions	% mut
	G/C : A/T	transitions : transversions	G to A C to T	G to T/C C to A/G	at **G**YW /WR**C**	A to G T to C	A to T/C T to A/G	at W**A** /T**W**
wt TDG^KD	41.7 : 58.3	49.8 : 50.2	55.2	44.8	53.0	45.9	54.1	65.0
Pms2^−/−Ung^−/− (NT)	79.0 : 21.0	89.2 : 10.8	98.4	1.6	66.0	54.3	45.7	76.7
*Pms2^−/−Ung^−/−*MBD4^KD	75.0 : 25.0	84.2 : 15.8	98.9	1.1	59.5	40.3	59.7	72.4
*Pms2^−/−Ung^−/−*TDG^KD	83.3 : 16.7	89.4 : 10.6	97.2	2.8	68.4	50.4	49.6	73.9
*Pms2^−/−Ung^−/−*SMUG^KD	85.7 : 14.3	91.3 : 8.7	98.8	1.2	65.7	46.5	53.5	71.6
*Pms2^−/−Ung^−/−*TDG/SMUG^KD	92.0 : 8.0	94.4 : 5.6	99.3	0.7	67.4	38.1	61.9	69.0

Figure 5. **Impact of uracil glycosylase silencing on the mutation profile of *Pms2^−/−Ung^−/−* GC B cells.** (A) Analysis of mutations in J_H4 intronic sequences from *Pms2^−/−Ung^−/−* splenic GC B cells (B220+GL7+CD95+) silenced for *Mbd4*, *Tdg*, *Smug1*, or both *Tdg* and *Smug1*, as well as *Tdg*-silenced WT cells. NT represents control cells isolated from bone marrow of *Pms2^−/−Ung^−/−* mice that were cultivated in the same conditions but not transduced before injection in *Rag2^−/−* recipient mice. KD, knockdown. (B) Pattern of nucleotide substitution for all the genotypes, corrected for base composition. No significant differences for frequencies of GYW/WR(C) or WA/TW hotspot mutations were observed for comparisons of values from individual mice with NT controls (two-tailed Mann Whitney *U* test). (C) Mutagenesis at A-T base pairs (percentage). Efficiency of knockdown in the analyzed GFP+ GC B cells compared with GFP− GC B cells is represented by a color code. Silencing of *Tdg* was achieved with two different shRNA sequences, represented by dots or triangles. **, P = 0.0012 (TDG^KD vs. NT) or 0.0061 (TGD/SMUG^KD vs. TDG^KD); two-tailed Mann-Whitney *U* test. All restored mice (three to seven for each antisense transduction), analyzed individually for glycosylase inhibition and J_H4 mutations, are represented.

DISCUSSION

The first observation of our work is that uracils generated by AID in the G1 phase can generate the complete spectrum of mutations observed in normal conditions at the Ig locus. These results are in good agreement with a similar study performed by Sharbeen et al. (2012), in which cell cycle restriction of Ugi, a specific inhibitor of UNG, could interfere with uracil excision only when expressed in G1. These two sets of data appear to favor a model in which UNG and MMR would operate within a similar time frame. The concomitant action of the two repair pathways suggests that they could cooperate to generate mutations at A-T base pairs.

UNG and APEX were proposed to help the MMR pathway for A-T mutagenesis by providing the DNA incision required for ExoI-mediated DNA resection and subsequent error-prone synthesis by Pol η (Schanz et al., 2009). However, even though some data supported the existence of this synergy at A-T bases (Frieder et al., 2009; Stavnezer et al., 2014; Zivojnovic et al., 2014), A-T mutations are hardly affected in *Ung^−/−* mice, which means that UNG is largely

dispensable for these types of mutations. Now, our work sheds new light on the hypothesis of UNG and MMR cooperation. The 50% reduction of A-T SHM that we observed in double-deficient $Ung^{-/-}Pms2^{-/-}$ mice establishes that the Pms2/Mlh1 complex can contribute to SHM, contrary to the model that prevailed for almost two decades (Frey et al., 1998; Phung et al., 1999; Ehrenstein et al., 2001; van Oers et al., 2010; Chahwan et al., 2012). This observation, combined with the almost complete disappearance of residual A-T mutations after further ablation of the uracil glycosylases SMUG1 and TDG, allows us to propose the following scenario (Fig. 6). UNG would support MMR-mediated A-T mutagenesis, most likely by attacking one uracil together with APEX2 (Stavnezer et al., 2014), which would create a nick for ExoI entry in the vicinity of a second uracil detected as a U:G mismatch by Msh2/Msh6 (Fig. 6 A). Nevertheless, loss of function of Ung would have little impact on A-T SHM because the nick could also be provided by Pms2/Mlh1, the genuine endonuclease of MMR, and by two additional uracil glycosylases, SMUG1, as described previously (Dingler et al., 2014), and TDG (Fig. 6 A), whose role in hypermutation had not been assessed so far. Around 8% of A-T mutations are still observed in our quadruple deficient mice ($Ung^{-/-}Pms2^{-/-}$ with silencing of Tdg and $Smug1$). Because inhibition of Tdg and $Smug1$ by RNAi was not complete, it is likely that nearly all A-T mutations are generated from nicks created by one of these four enzymes.

Inactivation of the endonuclease activity of Pms2 would be required to strictly confirm the catalytic role of Pms2 in this process, as an indirect contribution, such as a structural role in the assembly of protein repair complexes, could also be envisioned. However, we do not favor this hypothesis because the inactivation of Pms2 not only affects A-T mutagenesis in the context of UNG deficiency, but also alters the A over T mutation ratio in both the single $Pms2^{-/-}$ and the double $Ung^{-/-}Pms2^{-/-}$ configurations (Zivojnovic et al., 2014 and this study). Such a change in strand bias appears more readily explainable by an intrinsic bias in the DNA strand incised, rather than by an indirect scaffolding function. Moreover, this strand bias allows us to further propose that, instead of achieving simple backups for a dominant function, both uracil glycosylases and Pms2 contribute to the physiological process. Taking into account the intrinsic mutagenic profile of Pol η (a fourfold higher mutation frequency when copying T's rather than A's; Zivojnovic et al., 2014) and the 1.8-fold A over T bias observed in the mutation profile of V genes in the normal situation, one can indeed estimate the relative contribution of each pathway: the Pms2/Mlh1 complex would contribute to SHM under basal conditions and provide nicks in an unbiased fashion on both DNA strands, whereas uracil glycosylase–dependent nicks would be preferentially located on the nontranscribed/coding strand, both pathways contributing equally to A-T mutagenesis, with their distinct strand bias reflected in the global mutation profile (Fig. 6 B). Along this line, at least part of A-T mutations are generated through
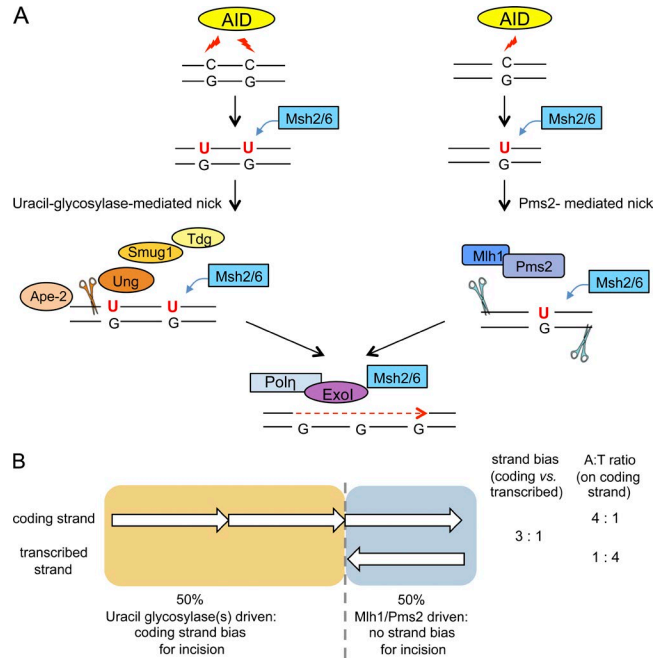
Figure 6. **A model whereby both uracil glycosylases and the Pms2/Mlh1 complex enable A–T base pair mutagenesis with a distinct strand bias.** (A) Overlapping enzymatic activities generate entry sites for ExoI in MMR-mediated A-T mutagenesis. (Right) Recognition of AID deamination products by Msh2–Msh6 stimulates the endonuclease activity of the Pms2–Mlh1 complex, which acts at distance on either DNA strands. (Left) In a situation of processive deamination, nicks introduced by uracil glycosylase–mediated base excision (UNG, SMUG1, and TDG) and APEX2 strand incision can participate in MMR-mediated error-prone repair. Glycosylases may also act in the context of two independent deamination events on both DNA strands or, possibly, in the context of a single uracil (see Discussion). (B) Pms2 versus uracil glycosylase contribution estimated from A/T mutation ratios. The 1.8- to twofold A over T ratio observed in hypermutation was estimated to correspond to a 3:1 strand bias in error-prone DNA synthesis, taking into account the intrinsic T over A mutation preference of Pol η (a 4:1 higher mutation frequency opposite T than opposite A; Zivojnovic et al., 2014). This strand bias is represented by arrows of unequal length, representing the relative A:T mutagenic patch on each strand, without aiming at indicating whether the patch is shorter or less frequent on the transcribed strand or differently located on the locus. If one considers, from mutations observed in $Pms2^{-/-}$ mice, that uracil glycosylases operate mainly on the coding, nontranscribed strand and that PMS2 endonuclease operates without strand bias and is responsible for most mutations introduced in the transcribed strand, both pathways appear to contribute equally to the generation of Msh2/6-driven A-T mutations.

a Pms2-independent pathway because the frequency of A-T mutations is reduced in $Ung^{-/-}Smug1^{-/-}$ mice (Dingler et al., 2014), as well as in $Ung^{-/-}Apex2^{-/-}$ mice (Stavnezer et al., 2014). Whereas the initial proposition of Schanz et al. (2009) (depicted in Fig. 6 A, left) involved two deamination events taking place in a processive manner along the nontranscribed strand, other scenarios are possible, like two independent events on both strands or even incision of a single uracil by glycosylases after prior recognition by Msh2/Msh6 and for-

mation of a sliding clamp detaching the complex from the mismatched base (Gradia et al., 1999). This last configuration could be privileged in the absence of Pms2 and compensate for its function. Whatever the configuration, the A over T ratio of 4 observed upon Pms2 deficiency argues for a preferential bias toward the nontranscribed, possibly more exposed strand for glycosylase attacks.

An explanation for such division of tasks between base excision repair and MMR pathways could be that Pms2/Mlh1 endonuclease activity may have limited efficiency in the G1 phase because of the absence of preexisting strand discontinuities. Indeed, under physiological conditions, Pms2/Mlh1 is not able to nick relaxed covalently closed double-stranded DNA, unless some structural anomalies such as bubbles are present in the DNA to allow for PCNA loading (Pluciennik et al., 2010; Kadyrova and Kadyrov, 2016). Whether such bubbles could be temporarily created by transcription or specific chromatin organization of the Ig locus remains an open question. Among uracil glycosylases, UNG clearly has a privileged function in SHM because TDG and SMUG1 cannot fully compensate for the simultaneous loss of function of *Ung* and *Pms2* (Fig. 5). Finally, the recruitment of SMUG1 and TDG appears to be mediated by the Msh2/Msh6 complex and restricted to the A–T pathway, as no processing of AID-induced uracils is observed in an Msh2 × UNG–deficient context (Rada et al., 2004).

Although our data do not allow us to rule out that some mutations at A-T bases occur during S or G2 phases, theoretical and experimental evidence supports the predominant role of the G1 phase in SHM. A recent study that was based on AID–Fucci fusion proteins similar to those used in the present article showed that nuclear AID is more stable and better tolerated in the G1 phase (Le and Maizels, 2015); thus, AID is more likely to introduce uracils before replication. Moreover, replicative DNA polymerases and dNTP are scarce in G1, which could slow down MMR gap filling and favor PCNA ubiquitination (Bak et al., 2014). This model is attractive, but the ncMMR pathway seems to be shared by many cell types, whereas MMR-mediated A–T mutagenesis during SHM is very specific to GC B cells in vivo. Indeed, although AID expression is mutagenic, it very poorly induces hypermutation at A–T base pairs in fibroblasts (Yoshikawa et al., 2002) or even in B cells activated in vitro with signals that mimic the GC environment (Nojima et al., 2011). What intrinsic property of in vivo GC B cells enables A–T hypermutation is still unknown, but the identification of new partners involved, reported in this study, may help to address this issue.

MATERIALS AND METHODS
Mouse strains
Aicda$^{-/-}$ mice were provided by T. Honjo (Kyoto University, Kyoto, Japan) and backcrossed against the C57BL/6 background for nine generations. Rag2(B6)–deficient mice were obtained from the Transgenesis and Archiving of Animal Models laboratory. *Ung*$^{-/-}$ and *Pms2*$^{-/-}$ mice were obtained from

D. Barnes (Clare Hall Laboratories, South Mimms, England, UK) and M. Liskay (Oregon Health and Science University, Portland, OR), respectively. *Ung*$^{-/-}$ mice were subjected to six to eight backcrosses with C57BL/6 and *Pms2*$^{-/-}$ mice to two to three backcrosses, before they were bred to generate double-deficient animals, which required a recombination event between these two loci located 29.8 Mb apart on chromosome 5. WT littermates of *Ung*$^{+/-}$ or *Pms2*$^{+/-}$ breedings were used for comparison with Pms2-, UNG-, and double-deficient animals. To generate UNG/Msh2/AID triple-deficient animals, the AID-Cre-ERT2 line was used (Dogan et al., 2009) because of local constraints for mouse line availability. The AID-Cre-ERT2 line has been bred with C57BL/6 since its generation in 2005. C57BL/6 mice were purchased from Charles River for *Tdg*-silencing experiments in WT HSCs. All experiments and procedures were approved by the ethics committee of Paris-Descartes University and authorized by the French Ministry of Research.

Construction of retroviral vectors
Mouse AID cDNA was amplified with use of a reverse primer containing a sequence coding for a $(G_4S)_3$ flexible linker and inserted in the EcoRI/HindIII sites of the pFucci–G1 orange plasmid (MBL International) to create AID-mKO$_2$-hCDT1. Then, AID-mKO$_2$-hCDT1 was reamplified and cloned in the EcoRI site of the pMIG retroviral vector (entry 9044; Addgene). AID-mCherry-geminin was assembled by PCR with AID-mKO2-hCDT1, pmCherrry (Takara Bio Inc.), and pFucci-G2 green (MBL International) as templates and then cloned in the BglII/EcoRI sites of pMIG. AID-fusion proteins with mutated degrons were created by site-directed mutagenesis PCR. All PCRs were performed with Phusion DNA polymerase (New England Biolabs, Inc.) with the primers listed in Tables S1 and S2.

A silencing cassette was derived from the BLOCK-iT PolII miR RNAi Expression system with the EmGFP kit (Thermo Fisher Scientific). A double-stranded sequence containing two BbsI restriction sites in a head-to-tail orientation was cloned in pcDNA6.2-GW/EmGFP-miR plasmid between the 5′ and 3′ miR–155 flanking sequences embedded in the 3′ untranslated region of EmGFP. Then, this modified cassette was amplified by PCR using forward and reverse primers that contained EcoRI and XhoI sites, respectively, and cloned in the EcoRI and SalI sites of the pMIG vector to replace the original IRES-EGFP sequence.

shRNA sequences, listed in Tables S1 and S2, were chosen using BLOCK-iT RNAi Designer (Thermo Fisher Scientific). Single-strand oligonucleotides with 5′-protruding ends were annealed and inserted in the BbsI sites according to the manufacturer's recommendation (Thermo Fisher Scientific).

Production and titration of ecotropic retroviral particles
Nonreplicative ecotropic γ–retroviral particles were produced by transient lipofection (XtremeGene 9 DNA transfection reagent; Roche) of 293T cells grown in DMEM/F-12 sup-

plemented with 10% FCS (Hyclone) with pMIG, pLTR–env, and CMV-Gag/Pol vectors (ratio 2:1:1). At 48 h after transfection, viral supernatants were filtered through 0.45-μm Minisart High Flow filters (Sartorius) and concentrated on centrifugal filter units (100K Amicon Ultra 15; EMD Millipore) to obtain titers ranging from 3×10^7 to 2×10^8 TU/ml.

Measure of mRNA quantities by qRT–PCR

RNA and genomic DNA were extracted simultaneously from 50–200,000 sorted cells with an Allprep DNA/RNA Micro kit (QIAGEN), after prior homogenization of the samples with QIAshredder columns (QIAGEN). RNA purification included on-column incubation with DNase I (QIAGEN) to remove traces of genomic DNA. cDNA was synthesized by random priming with a multiple-temperature cDNA synthesis kit (AffinityScript; Agilent Technologies). Relative transcript abundance was assessed by real-time PCR on a PCR machine (7500 Fast System Real-Time; Applied Biosystems; 2 min at 50°C, 10 min at 95°C, and 40 cycles of 10 s at 95°C and 1 min at 60°C) in universal PCR master mix (No AmpErase UNG; Applied Biosystems), with the following validated TaqMan assays: Mm00437762_m1 (β2-microglobulin), Mm01225357_g1 (Tdg), Mm01184338_m1 (Mbd4), and Mm00452897_m1 (Smug1). Relative quantities were calculated by the ΔΔCt method using β2-microglobulin as a reference gene to normalize the RNA content.

HSC transduction and adoptive transfer experiments

HSCs were purified with the Mouse Lineage Cell Depletion kit (Miltenyi Biotec) from bone marrow of 8–12-wk-old mice and cultured for 48 h in DMEM supplemented with 15% heat-inactivated FCS (HyClone), 1 mM Na-pyruvate, 10 ng/ml mouse IL-3 (mIL-3), 10 ng/ml mIL-6, 100 ng/ml mouse stem cell factor, 100 ng/ml mFlt3L, and 50 ng/ml human thrombopoietin (all cytokines are from PeproTech). 6-well plates (BD) were coated overnight at 4°C with 200 μl/cm^2 of a 50-μg/ml RetroNectin solution (Takara Bio Inc.) in PBS before retroviral loading for 4 h at 37°C in the presence of 4 μg/ml polybrene (H9268; Sigma-Aldrich). Lin$^−$ cells were incubated for 4 h at 37°C in virus-bound wells at 10^6 cells/ml, detached by manual rubbing, washed twice, resuspended in PBS, and injected ($1–2 \times 10^6$ cells in 200 μl) through the retroorbital sinus in 8–20-wk-old Rag2(B6)–deficient mice irradiated 8 h before transfer (4.5 Gy; RS-2000 X-Ray; RadSource Technologies).

Flow cytometry analysis and cell sorting

The following antibodies were used: B220 APC-e780 (clone RA3-6B2; eBioscience), GL7 Alexa Fluor 647 (clone GL7; eBioscience), GL7 e-450 (clone GL7; eBioscience), PNA biotin (Vector Laboratories), streptavidin PE-Cy7 (eBioscience), and CD95 PE-Cy7 (clone Jo2; BD). Dead cells were excluded by staining with SytoxBlue (Invitrogen). Two-dimensional cell-cycle analysis of Lin$^−$ cells involved S-phase labeling with the APC BrdU Flow kit (BD), followed by DNA

staining with 3 μM DAPI staining solution (DAPI hydrochloride; Invitrogen) for 15 min at 25°C. For one-dimensional cell cycle analysis of in vitro–activated B cells, 10^6 cells/ml were incubated for 30 min at 37°C in a 2-μM Hoechst 33342 solution (Invitrogen) in DMEM. Cytometry profiles were acquired with an LSR Fortessa cytometer (BD) equipped with 355-nm and 561-nm lasers, and data were analyzed with Diva (BD) and FlowJo (Tree Star) softwares. Cells were sorted on a FACSAria I cell sorter (BD).

Immunization, genomic DNA extraction, and sequence analysis

For each immunization, 5×10^9 SRBCs (Eurobio) were washed three times in PBS, resuspended in 500 μl of PBS, and injected intraperitoneally. 14 d after primary immunization or 5 d after secondary immunization, B220$^+$PNA^{high}GL7$^+$ (or B220$^+$CD95$^+$GL7$^+$) splenocytes were sorted, and the J$_H$4 intron flanking rearranged V$_H$ sequences was amplified with a mixture of five V$_H$ primers designed to amplify most mouse V$_H$ families and a downstream primer allowing the determination of 443 bp of noncoding sequences downstream of rearranged J$_H$4 segments (461 bp for AID-restriction experiments), as previously described (Delbos et al., 2005). Mutations reported for Ung-, Pms2-, and Ung × Pms2–deficient mice were determined from B220$^+$CD95$^+$GL7$^+$ B cells isolated from Peyer's patches of 4-mo-old animals. Mutations were detected with use of CodonCode Aligner (CodonCode Corporation), and two types of analyses were performed: first, only identical sequences were removed, and second, repeated mutations were counted only once when three or more mutations were found in multiple sequences sharing the same CDR3 (clonal relationship) or not (putative PCR hybrids). Both analyses gave similar mutation profiles.

In vitro B cell activation

In total, 5×10^5 B220$^+$EGFP$^+$GL7$^−$PNA^{low} B cells from restored SRBC-immunized animals were resuspended at 10^6 cells/ml in RPMI complete medium (FCS 15%, 0.1 mM β-mercaptoethanol, 20 mM Hepes, 1 mM Na-pyruvate, and nonessential amino acids) supplemented with 20 μg/ml Salmonella typhimurium LPS (Sigma-Aldrich) and 25 ng/ml mouse recombinant IL-4 (eBioscience). Cells were cultured for 3 d at a density <10^6 cells/ml before cell cycle analysis.

Online supplemental material

Table S1 lists primers for cell cycle–restricted AID constructs. Table S2 lists primers for shRNA constructs.

REFERENCES

Bak, S.T., D. Sakellariou, and J. Pena-Diaz. 2014. The dual nature of mismatch repair as antimutator and mutator: for better or for worse. *Front. Genet.* 5:287. http://dx.doi.org/10.3389/fgene.2014.00287

Bardwell, P.D., A. Martin, E. Wong, Z. Li, W. Edelmann, and M.D. Scharff. 2003. Cutting edge: the G-U mismatch glycosylase methyl-CpG binding domain 4 is dispensable for somatic hypermutation and class switch recombination. *J. Immunol.* 170:1620–1624. http://dx.doi.org/10.4049/jimmunol.170.4.1620

Berek, C., and C. Milstein. 1987. Mutation drift and repertoire shift in the maturation of the immune response. *Immunol. Rev.* 96:23–41. http://dx.doi.org/10.1111/j.1600-065X.1987.tb00507.x

Chahwan, R., J.M. van Oers, E. Avdievich, C. Zhao, W. Edelmann, M.D. Scharff, and S. Roa. 2012. The ATPase activity of MLH1 is required to orchestrate DNA double-strand breaks and end processing during class switch recombination. *J. Exp. Med.* 209:671–678. http://dx.doi.org/10.1084/jem.20111531

Cortázar, D., C. Kunz, J. Selfridge, T. Lettieri, Y. Saito, E. MacDougall, A. Wirz, D. Schuermann, A.L. Jacobs, F. Siegrist, et al. 2011. Embryonic lethal phenotype reveals a function of TDG in maintaining epigenetic stability. *Nature.* 470:419–423. http://dx.doi.org/10.1038/nature09672

Delbos, F., A. De Smet, A. Faili, S. Aoufouchi, J.C. Weill, and C.A. Reynaud. 2005. Contribution of DNA polymerase η to immunoglobulin gene hypermutation in the mouse. *J. Exp. Med.* 201:1191–1196. http://dx.doi.org/10.1084/jem.20050292

Delbos, F., S. Aoufouchi, A. Faili, J.C. Weill, and C.A. Reynaud. 2007. DNA polymerase η is the sole contributor of A/T modifications during immunoglobulin gene hypermutation in the mouse. *J. Exp. Med.* 204:17–23. http://dx.doi.org/10.1084/jem.20062131

Dingler, F.A., K. Kemmerich, M.S. Neuberger, and C. Rada. 2014. Uracil excision by endogenous SMUG1 glycosylase promotes efficient Ig class switching and impacts on A:T substitutions during somatic mutation. *Eur. J. Immunol.* 44:1925–1935. http://dx.doi.org/10.1002/eji.201444482

Di Noia, J.M., and M.S. Neuberger. 2007. Molecular mechanisms of antibody somatic hypermutation. *Annu. Rev. Biochem.* 76:1–22. http://dx.doi.org/10.1146/annurev.biochem.76.061705.090740

Dogan, I., B. Bertocci, V. Vilmont, F. Delbos, J. Mégret, S. Storck, C.A. Reynaud, and J.C. Weill. 2009. Multiple layers of B cell memory with different effector functions. *Nat. Immunol.* 10:1292–1299. http://dx.doi.org/10.1038/ni.1814

Ehrenstein, M.R., C. Rada, A.M. Jones, C. Milstein, and M.S. Neuberger. 2001. Switch junction sequences in PMS2-deficient mice reveal a microhomology-mediated mechanism of Ig class switch recombination. *Proc. Natl. Acad. Sci. USA.* 98:14553–14558. http://dx.doi.org/10.1073/pnas.241525998

Frey, S., B. Bertocci, F. Delbos, L. Quint, J.C. Weill, and C.A. Reynaud. 1998. Mismatch repair deficiency interferes with the accumulation of mutations in chronically stimulated B cells and not with the hypermutation process. *Immunity.* 9:127–134. http://dx.doi.org/10.1016/S1074-7613(00)80594-4

Frieder, D., M. Larijani, C. Collins, M. Shulman, and A. Martin. 2009. The concerted action of Msh2 and UNG stimulates somatic hypermutation at A • T base pairs. *Mol. Cell. Biol.* 29:5148–5157. http://dx.doi.org/10.1128/MCB.00647-09

Gitlin, A.D., Z. Shulman, and M.C. Nussenzweig. 2014. Clonal selection in the germinal centre by regulated proliferation and hypermutation. *Nature.* 509:637–640. http://dx.doi.org/10.1038/nature13300

Gitlin, A.D., C.T. Mayer, T.Y. Oliveira, Z. Shulman, M.J. Jones, A. Koren, and M.C. Nussenzweig. 2015. T cell help controls the speed of the cell cycle in germinal center B cells. *Science.* 349:643–646. http://dx.doi.org/10.1126/science.aac4919

Goellner, E.M., C.D. Putnam, and R.D. Kolodner. 2015. Exonuclease 1-dependent and independent mismatch repair. *DNA Repair (Amst.).* 32:24–32. http://dx.doi.org/10.1016/j.dnarep.2015.04.010

Gradia, S., D. Subramanian, T. Wilson, S. Acharya, A. Makhov, J. Griffith, and R. Fishel. 1999. hMSH2–hMSH6 forms a hydrolysis-independent sliding clamp on mismatched DNA. *Mol. Cell.* 3:255–261. http://dx.doi.org/10.1016/S1097-2765(00)80316-0

Hombauer, H., A. Srivatsan, C.D. Putnam, and R.D. Kolodner. 2011. Mismatch repair, but not heteroduplex rejection, is temporally coupled to DNA replication. *Science.* 334:1713–1716. http://dx.doi.org/10.1126/science.1210770

Imai, K., G. Slupphaug, W.I. Lee, P. Revy, S. Nonoyama, N. Catalan, L. Yel, M. Forveille, B. Kavli, H.E. Krokan, et al. 2003. Human uracil–DNA glycosylase deficiency associated with profoundly impaired immunoglobulin class-switch recombination. *Nat. Immunol.* 4:1023–1028. http://dx.doi.org/10.1038/ni974

Jansen, J.G., P. Langerak, A. Tsaalbi-Shtylik, P. van den Berk, H. Jacobs, and N. de Wind. 2006. Strand-biased defect in C/G transversions in hypermutating immunoglobulin genes in Rev1-deficient mice. *J. Exp. Med.* 203:319–323. http://dx.doi.org/10.1084/jem.20052227

Kadyrov, F.A., L. Dzantiev, N. Constantin, and P. Modrich. 2006. Endonucleolytic function of MutLα in human mismatch repair. *Cell.* 126:297–308. http://dx.doi.org/10.1016/j.cell.2006.05.039

Kadyrova, L.Y., and F.A. Kadyrov. 2016. Endonuclease activities of MutLα and its homologs in DNA mismatch repair. *DNA Repair (Amst.).* 38:42–49. http://dx.doi.org/10.1016/j.dnarep.2015.11.023

Krijger, P.H., A. Tsaalbi-Shtylik, N. Wit, P.C. van den Berk, N. de Wind, and H. Jacobs. 2013. Rev1 is essential in generating G to C transversions downstream of the Ung2 pathway but not the Msh2+Ung2 hybrid pathway. *Eur. J. Immunol.* 43:2765–2770. http://dx.doi.org/10.1002/eji.201243191

Kunkel, T.A., and D.A. Erie. 2015. Eukaryotic mismatch repair in relation to DNA replication. *Annu. Rev. Genet.* 49:291–313. http://dx.doi.org/10.1146/annurev-genet-112414-054722

Langerak, P., A.O. Nygren, P.H. Krijger, P.C. van den Berk, and H. Jacobs. 2007. A/T mutagenesis in hypermutated immunoglobulin genes strongly depends on PCNAK164 modification. *J. Exp. Med.* 204:1989–1998. http://dx.doi.org/10.1084/jem.20070902

Le, Q., and N. Maizels. 2015. Cell cycle regulates nuclear stability of AID and determines the cellular response to AID. *PLoS Genet.* 11:e1005411. http://dx.doi.org/10.1371/journal.pgen.1005411

Li, S., Y. Zhao, and J.Y. Wang. 2013. Analysis of Ig gene hypermutation in $Ung^{-/-}Polh^{-/-}$ mice suggests that UNG and A:T mutagenesis pathway target different U:G lesions. *Mol. Immunol.* 53:214–217. http://dx.doi.org/10.1016/j.molimm.2012.08.009

Liu, M., and D.G. Schatz. 2009. Balancing AID and DNA repair during somatic hypermutation. *Trends Immunol.* 30:173–181. http://dx.doi.org/10.1016/j.it.2009.01.007

Liu, E., X. Li, F. Yan, Q. Zhao, and X. Wu. 2004. Cyclin-dependent kinases phosphorylate human Cdt1 and induce its degradation. *J. Biol. Chem.* 279:17283–17288. http://dx.doi.org/10.1074/jbc.C300549200

McGarry, T.J., and M.W. Kirschner. 1998. Geminin, an inhibitor of DNA replication, is degraded during mitosis. *Cell.* 93:1043–1053. http://dx.doi.org/10.1016/S0092-8674(00)81209-X

Muramatsu, M., K. Kinoshita, S. Fagarasan, S. Yamada, Y. Shinkai, and T. Honjo. 2000. Class switch recombination and hypermutation require activation-induced cytidine deaminase (AID), a potential RNA editing enzyme. *Cell.* 102:553–563. http://dx.doi.org/10.1016/S0092-8674(00)00078-7

Nojima, T., K. Haniuda, T. Moutai, M. Matsudaira, S. Mizokawa, I. Shiratori, T. Azuma, and D. Kitamura. 2011. In-vitro derived germinal centre B cells differentially generate memory B or plasma cells in vivo. *Nat. Commun.* 2:465. http://dx.doi.org/10.1038/ncomms1475

Pear, W.S., J.P. Miller, L. Xu, J.C. Pui, B. Soffer, R.C. Quackenbush, A.M. Pendergast, R. Bronson, J.C. Aster, M.L. Scott, and D. Baltimore. 1998. Efficient and rapid induction of a chronic myelogenous leukemia-like myeloproliferative disease in mice receiving P210 bcr/abl-transduced bone marrow. *Blood.* 92:3780–3792.

Peña-Diaz, J., S. Bregenhorn, M. Ghodgaonkar, C. Follonier, M. Artola-Borán, D. Castor, M. Lopes, A.A. Sartori, and J. Jiricny. 2012. Noncanonical mismatch repair as a source of genomic instability in human cells. *Mol. Cell.* 47:669–680. http://dx.doi.org/10.1016/j.molcel.2012.07.006

Pham, P., R. Bransteitter, J. Petruska, and M.F. Goodman. 2003. Processive AID-catalysed cytosine deamination on single-stranded DNA simulates somatic hypermutation. *Nature.* 424:103–107. http://dx.doi.org/10.1038/nature01760

Phung, Q.H., D.B. Winter, R. Alrefai, and P.J. Gearhart. 1999. Hypermutation in IgV genes from mice deficient in the MLH1 mismatch repair protein. *J. Immunol.* 162:3121–3124.

Pluciennik, A., L. Dzantiev, R.R. Iyer, N. Constantin, F.A. Kadyrov, and P. Modrich. 2010. PCNA function in the activation and strand direction of MutLα endonuclease in mismatch repair. *Proc. Natl. Acad. Sci. USA.* 107:16066–16071. http://dx.doi.org/10.1073/pnas.1010662107

Rada, C., M.R. Ehrenstein, M.S. Neuberger, and C. Milstein. 1998. Hot spot focusing of somatic hypermutation in MSH2-deficient mice suggests two stages of mutational targeting. *Immunity.* 9:135–141. http://dx.doi.org/10.1016/S1074-7613(00)80595-6

Rada, C., G.T. Williams, H. Nilsen, D.E. Barnes, T. Lindahl, and M.S. Neuberger. 2002. Immunoglobulin isotype switching is inhibited and somatic hypermutation perturbed in UNG-deficient mice. *Curr. Biol.* 12:1748–1755. http://dx.doi.org/10.1016/S0960-9822(02)01215-0

Rada, C., J.M. Di Noia, and M.S. Neuberger. 2004. Mismatch recognition and uracil excision provide complementary paths to both Ig switching and the A/T-focused phase of somatic mutation. *Mol. Cell.* 16:163–171. http://dx.doi.org/10.1016/j.molcel.2004.10.011

Revy, P., T. Muto, Y. Levy, F. Geissmann, A. Plebani, O. Sanal, N. Catalan, M. Forveille, R. Dufourcq-Labelouse, A. Gennery, et al. 2000. Activation-induced cytidine deaminase (AID) deficiency causes the autosomal recessive form of the hyper-IgM syndrome (HIGM2). *Cell.* 102:565–575. http://dx.doi.org/10.1016/S0092-8674(00)00079-9

Reynaud, C.A., F. Delbos, A. Faili, Q. Guéranger, S. Aoufouchi, and J.C. Weill. 2009. Competitive repair pathways in immunoglobulin gene hypermutation. *Philos. Trans. R. Soc. Lond. B Biol. Sci.* 364:613–619. http://dx.doi.org/10.1098/rstb.2008.0206

Sakaue-Sawano, A., H. Kurokawa, T. Morimura, A. Hanyu, H. Hama, H. Osawa, S. Kashiwagi, K. Fukami, T. Miyata, H. Miyoshi, et al. 2008. Visualizing spatiotemporal dynamics of multicellular cell-cycle progression. *Cell.* 132:487–498. http://dx.doi.org/10.1016/j.cell.2007.12.033

Schanz, S., D. Castor, F. Fischer, and J. Jiricny. 2009. Interference of mismatch and base excision repair during the processing of adjacent U/G mispairs may play a key role in somatic hypermutation. *Proc. Natl. Acad. Sci. USA.* 106:5593–5598. http://dx.doi.org/10.1073/pnas.0901726106

Sharbeen, G., C.W. Yee, A.L. Smith, and C.J. Jolly. 2012. Ectopic restriction of DNA repair reveals that UNG2 excises AID-induced uracils predominantly or exclusively during G1 phase. *J. Exp. Med.* 209:965–974. http://dx.doi.org/10.1084/jem.20112379

Stavnezer, J., E.K. Linehan, M.R. Thompson, G. Habboub, A.J. Ucher, T. Kadungure, D. Tsuchimoto, Y. Nakabeppu, and C.E. Schrader. 2014. Differential expression of APE1 and APE2 in germinal centers promotes error-prone repair and A:T mutations during somatic hypermutation. *Proc. Natl. Acad. Sci. USA.* 111:9217–9222. http://dx.doi.org/10.1073/pnas.1405590111

van Oers, J.M., S. Roa, U. Werling, Y. Liu, J. Genschel, H. Hou Jr., R.S. Sellers, P. Modrich, M.D. Scharff, and W. Edelmann. 2010. PMS2 endonuclease activity has distinct biological functions and is essential for genome maintenance. *Proc. Natl. Acad. Sci. USA.* 107:13384–13389. http://dx.doi.org/10.1073/pnas.1008589107

Victora, G.D., and M.C. Nussenzweig. 2012. Germinal centers. *Annu. Rev. Immunol.* 30:429–457. http://dx.doi.org/10.1146/annurev-immunol-020711-075032

Visnes, T., B. Doseth, H.S. Pettersen, L. Hagen, M.M. Sousa, M. Akbari, M. Otterlei, B. Kavli, G. Slupphaug, and H.E. Krokan. 2009. Uracil in DNA and its processing by different DNA glycosylases. *Philos. Trans. R. Soc. Lond. B Biol. Sci.* 364:563–568. http://dx.doi.org/10.1098/rstb.2008.0186

Weill, J.C., and C.A. Reynaud. 2008. DNA polymerases in adaptive immunity. *Nat. Rev. Immunol.* 8:302–312. http://dx.doi.org/10.1038/nri2281

Yoshikawa, K., I.M. Okazaki, T. Eto, K. Kinoshita, M. Muramatsu, H. Nagaoka, and T. Honjo. 2002. AID enzyme-induced hypermutation in an actively transcribed gene in fibroblasts. *Science.* 296:2033–2036. http://dx.doi.org/10.1126/science.1071556

Zanotti, K.J., and P.J. Gearhart. 2016. Antibody diversification caused by disrupted mismatch repair and promiscuous DNA polymerases. *DNA Repair (Amst.).* 38:110–116. http://dx.doi.org/10.1016/j.dnarep.2015.11.011

Zeng, X., D.B. Winter, C. Kasmer, K.H. Kraemer, A.R. Lehmann, and P.J. Gearhart. 2001. DNA polymerase η is an A-T mutator in somatic hypermutation of immunoglobulin variable genes. *Nat. Immunol.* 2:537–541. http://dx.doi.org/10.1038/88740

Zivojnovic, M., F. Delbos, G. Girelli Zubani, A. Julé, A. Alcais, J.C. Weill, C.A. Reynaud, and S. Storck. 2014. Somatic hypermutation at A/T-rich oligonucleotide substrates shows different strand polarities in Ung-deficient or -proficient backgrounds. *Mol. Cell. Biol.* 34:2176–2187. http://dx.doi.org/10.1128/MCB.01452-13

Zlatanou, A., E. Despras, T. Braz-Petta, I. Boubakour-Azzouz, C. Pouvelle, G.S. Stewart, S. Nakajima, A. Yasui, A.A. Ishchenko, and P.L. Kannouche. 2011. The hMsh2-hMsh6 complex acts in concert with monoubiquitinated PCNA and Pol η in response to oxidative DNA damage in human cells. *Mol. Cell.* 43:649–662. http://dx.doi.org/10.1016/j.molcel.2011.06.023

1180

Multiple uracil-repair pathways for A-T SHM | Girelli Zubani et al.